Received: 27 July 2021 | Revised: 18 October 2021 | Accepted: 16 November 2021

DOI: 10.1111/nan.12784

ORIGINAL ARTICLE

Neuropathology and Applied Neurobiology
JOURNAL OF THE BRITISH NEUROPATHOLOGICAL SOCIETY

WILEY

The desmin mutation R349P increases contractility and fragility of stem cell-generated muscle micro-tissues

Marina Spörrer[1] | Delf Kah[1] | Richard C. Gerum[1] | Barbara Reischl[2] | Danyil Huraskin[3] | Claire A. Dessalles[1,4] | Werner Schneider[1] | Wolfgang H. Goldmann[1,5] | Harald Herrmann[5,6] | Ingo Thievessen[1,5] | Christoph S. Clemen[7,8] | Oliver Friedrich[2,5] | Said Hashemolhosseini[3,5] | Rolf Schröder[5,6] | Ben Fabry[1,5]

[1]Biophysics Group, Department of Physics, Friedrich-Alexander University Erlangen-Nuremberg (FAU), Erlangen, Germany

[2]Institute of Medical Biotechnology, Department of Chemical and Biological Engineering, FAU, Erlangen, Germany

[3]Institute of Biochemistry, Medical Faculty, FAU, Erlangen, Germany

[4]LadHyX, CNRS, Ecole Polytechnique, Institut Polytechnique de Paris, Palaiseau, France

[5]Muscle Research Center Erlangen (MURCE), FAU, Erlangen, Germany

[6]Institute of Neuropathology, University Hospital Erlangen, FAU, Erlangen, Germany

[7]Institute of Aerospace Medicine, German Aerospace Center (DLR), Cologne, Germany

[8]Center for Physiology and Pathophysiology, Institute of Vegetative Physiology, Medical Faculty, University of Cologne, Cologne, Germany

Correspondence
Ben Fabry, Biophysics Group, Department of Physics, Friedrich-Alexander University Erlangen-Nuremberg (FAU), Erlangen, Germany.
Email: ben.fabry@fau.de

Funding information
Deutsche Forschungsgemeinschaft, Grant/Award Numbers: HA3309/7-1, HA3309/6-1, HA3309/3-1, FR-2993/23.1, FA-336/12.1, TRR 225 project 326998133 (subprojects A01, B08, and C02); Muscle Research Center Erlangen; Ecole Polytechnique

Abstract

Aims: Desminopathies comprise hereditary myopathies and cardiomyopathies caused by mutations in the intermediate filament protein desmin that lead to severe and often lethal degeneration of striated muscle tissue. Animal and single cell studies hinted that this degeneration process is associated with massive ultrastructural defects correlating with increased susceptibility of the muscle to acute mechanical stress. The underlying mechanism of mechanical susceptibility, and how muscle degeneration develops over time, however, has remained elusive.

Methods: Here, we investigated the effect of a desmin mutation on the formation, differentiation, and contractile function of in vitro-engineered three-dimensional micro-tissues grown from muscle stem cells (satellite cells) isolated from heterozygous R349P desmin knock-in mice.

Results: Micro-tissues grown from desmin-mutated cells exhibited spontaneous unsynchronised contractions, higher contractile forces in response to electrical stimulation, and faster force recovery compared with tissues grown from wild-type cells. Within 1 week of culture, the majority of R349P desmin-mutated tissues disintegrated, whereas wild-type tissues remained intact over at least three weeks. Moreover, under tetanic stimulation lasting less than 5 s, desmin-mutated tissues partially or completely ruptured, whereas wild-type tissues did not display signs of damage.

Conclusions: Our results demonstrate that the progressive degeneration of desmin-mutated micro-tissues is closely linked to extracellular matrix fibre breakage associated with increased contractile forces and unevenly distributed tensile stress. This suggests that the age-related degeneration of skeletal and cardiac muscle in patients suffering from desminopathies may be similarly exacerbated by mechanical damage from high-intensity muscle contractions. We conclude that micro-tissues may provide a valuable

Marina Spörrer and Delf Kah contributed equally to this work.

tool for studying the organization of myocytes and the pathogenic mechanisms of myopathies.

KEYWORDS
desmin, desminopathy, micro-tissue, skeletal muscle physiology, tissue engineering

INTRODUCTION

Desmin is the primary intermediate filament in skeletal, cardiac, and smooth muscle [1–4]. Desmin filaments form a scaffold around the myofibrillar Z-discs, connecting the contractile apparatus to the subsarcolemmal cytoskeleton, myo-nuclei, mitochondria, and other organelles. Thus, the desmin cytoskeletal network plays a central role in myofibrillar integrity and force transmission [1,2,4,5]. It is therefore not surprising that a number of desmin mutations lead to disturbed filament formation in particular under mechanical stress, impaired force transmission, and ultimately to myofibrillar degeneration [2,4,6,7]. A meta-analysis of 159 patients with desmin gene mutations reported that more than 70% of the patients developed myopathies, and 50% developed cardiomyopathies. Desminopathies are rare in humans (less than 50 cases per 100,000 individuals [4]) but are associated with severely reduced quality of life and life expectancy [2].

Over the last decades, our understanding of desminopathies has been greatly improved by the use of mouse models. Numerous studies have shown that mice either lacking wild-type desmin or expressing mutant desmin develop disorganised muscle fibres [8,9], desmin-positive aggregates [10], skeletal muscle weakness [10,11], increased muscle vulnerability during contraction [11], and mitochondrial dysfunction [8,12,13]. Other studies confirmed these results in zebrafish. Larvae carrying a desmin mutation were smaller than wild-type animals, their swimming activity was reduced, and their muscles showed structural disorganization [14]. Furthermore, disruption of the excitation-contraction (EC) coupling machinery and abnormal subcellular localization of ryanodine receptors (RyR) were detected in desmin-negative zebrafish [15].

Studies on NIH-3T3 fibroblasts transfected with the most common desmin mutation in humans, R350P, showed disrupted intermediate filament (IF) networks as well as cytoplasmic protein aggregates, which are in agreement with findings in animal studies [16]. However, these and other single cell studies have not provided insight into mechanisms that explain how cytoskeletal network disorganization and the presence of desmin-positive aggregates lead to muscle dysfunction at the tissue level. Moreover, a follow-up study found that several other desmin mutations that cause diseases in humans and animals did not alter filament formation at the single cell level [17].

To explore potential mechanisms that link desmin-related structural aberrations at the cellular level to the increased mechanical vulnerability and loss-of-function at the level of muscle tissue, we generated bioartificial three-dimensional (3-D) micro-tissues from desmin-mutated cells. We reasoned that such 3-D micro-tissues may better reproduce the in vivo situation compared with classical single cell studies, while at the same time being easier to handle and providing higher measurement throughput than whole muscle tissue or muscle fibres dissected from animals.

Key points

- Mutations in the intermediate filament desmin cause myopathies and cardiomyopathies associated with increased susceptibility of muscle tissue to mechanical stress.
- Micro-tissues grown from satellite cells from R349P desmin knock-in mice are a versatile in-vitro model for studying desminopathies.
- Tissues carrying the R349P desmin mutation exhibit higher and unevenly distributed contractile forces that lead to progressive disintegration of extracellular matrix fibres.

Our approach is based on a previously established micro-tissue system, where muscle cells are mixed with unpolymerized collagen-I and Matrigel in a small well containing two flexible pillars [18–20]. Upon polymerization of matrix proteins into a fibrillar network, the embedded cells begin to adhere, spread, and generate contractile forces. These forces compact the matrix network fibres, which wrap around and align between the flexible pillars. The cells in turn align with the parallel matrix fibre bundles, fuse, and over time form a 3-D contractile tissue. The force generation of this tissue can be measured by the deflection of the flexible pillars. 3-D micro-tissues grown from skeletal muscle cell sources can thus be used as a platform for studying physiological and mechanical properties of muscles [20,21], for drug testing [22,23], and for disease modelling [23–25].

As the cell source for generating micro-tissues, we used skeletal muscle stem cells (satellite cells) from wild-type mice and from mice carrying an R349P desmin mutation, which is the orthologue of the R350P mutation in humans. In addition, we added electrical stimulation electrodes to the 3-D culture system to measure both the static forces (baseline tone) and the active forces (contractile force in response to electrical stimulation) of the muscle micro-tissues. We found that micro-tissues grown from desmin-mutated satellite cells exhibited decreased static forces but increased active contractile forces compared with wild-type tissues, indicating pronounced hypercontractility. Furthermore, mutated tissues showed less organised fibre structures and were prone to tissue disintegration in response to tetanic electrical stimulation.

MATERIALS AND METHODS

Mice strains, skeletal muscle cell extractions, and culturing conditions

The R349P desmin knock-in mouse model (B6J.129Sv-*Des*$^{tm1.1Ccrs}$/Cscl MGI:5708562; hereafter "Des^{R349P}") was generated as previously described [10]. Mouse experiments were performed following animal welfare laws and approved by the responsible local committee (animal protection officer, Sachgebiet Tierschutzangelegenheiten, FAU Erlangen-Nürnberg, reference numbers: I/39/EE006, TS-07/11). Mice were housed in cages at 22 ± 1°C and relative humidity of 50–60% on a 12 h light/dark cycle. Water and food were provided ad libitum.

We prepared satellite cells from two wild-type (wt) BL6 mice and two heterozygous Des^{R349P} (hereafter "Des$^{wt/R349P}$") BL6 mice (age 2–3 months). Primary muscle satellite cells were extracted and pooled from 1–2 g of striated skeletal muscle tissue per mouse using the MACS Satellite Cell Isolation Kit (Miltenyi Biotech) according to the manufacturer's instructions [26]. Cells were seeded at a density of about 1000 cells/cm^2 in culture dishes (353003, Corning) coated with Matrigel. For this purpose, 1% Matrigel (Corning) in culture medium was applied to the dishes in a thin layer (10 µl of the solution per culture dish was spread with a cell scraper) and then incubated for 2 h at 37°C and 5% CO_2. The culture dishes could be used directly or stored with the addition of medium at incubation conditions. Culture medium consisted of Dulbecco's Modified Eagle Medium (DMEM, Gibco, 41966) supplemented with 40% (v/v) Ham's F10 nutrient mixture (Gibco), 20% (v/v) fetal calf serum, 1% (v/v) penicillin–streptomycin (Thermo Fisher, 15070, containing 10,000 units/ml of penicillin and 10,000 µg/ml of streptomycin) and 5 ng/ml recombinant human fibroblast growth factor (G5071, Promega).

Fabrication of 3-D micro-tissues

The protocol for fabricating 3-D muscle micro-tissues was adapted from Legant et al [18]. Tissues were grown in PDMS devices containing 18 small wells with dimensions of 3.6 × 1.8 × 2 mm (l × w × h) with two flexible pillars (diameter 500 µm, 2.5 mm height, 1.8 mm centre-to-centre distance) (Figure 1A). The PDMS chambers were coated with a solution of 1% Pluronic F-127 acid (Sigma-Aldrich) in water overnight to prevent matrix proteins from sticking to the walls of the PDMS chambers. After aspirating the coating solution, 6 µl of an unpolymerized ice-cold collagen-I/Matrigel solution was pipetted into each well. 1 ml of solution contained 100 µl of 2 mg/ml Collagen R (collagen I from rat tail veins, Matrix Bioscience, 50301), 77 µl of 5.2 mg/ml Collagen G (collagen I from bovine calf skin, Matrix Bioscience, 50104), 100 µl of 15 mg/ml Matrigel (Corning), 35.1 µl $NaHCO_3$ (23 mg/ml, Sigma-Aldrich), 35.1 µl 10× DMEM (Seraglob), 4.2 µl NaOH (1 M) and 649 µl of dilution medium that consisted of one volume part $NaHCO_3$ (23 mg/ml), one volume part 10× DMEM, and eight volume parts distilled H_2O, adjusted to pH 10 using NaOH. The PDMS devices were centrifuged (1 min at 300 g) and incubated at 37°C and 5% CO_2 for 1 h, during which the collagen-I/Matrigel solution polymerized. Next, a second layer of 6 µl unpolymerized ice-cold collagen-I/Matrigel solution mixed with 5000 cells was pipetted on top of the polymerized bottom layer in each PDMS chamber, allowing it to polymerize for 1 h at 37°C and 5% CO_2. Then, 1 ml of culture medium was carefully pipetted on top of the wells of each device.

Upon polymerization, the collagen-I/Matrigel solution forms a fibre network to which the skeletal muscle cells adhere, spread, and apply forces, causing a collective re-modelling of the network into a dense tissue with parallel bundles of fibres that span between the two pillars (Figure 2A). This process of tissue formation is completed typically within 12 h after seeding. 24 h after seeding, the culture medium was exchanged for a differentiation medium, which was changed

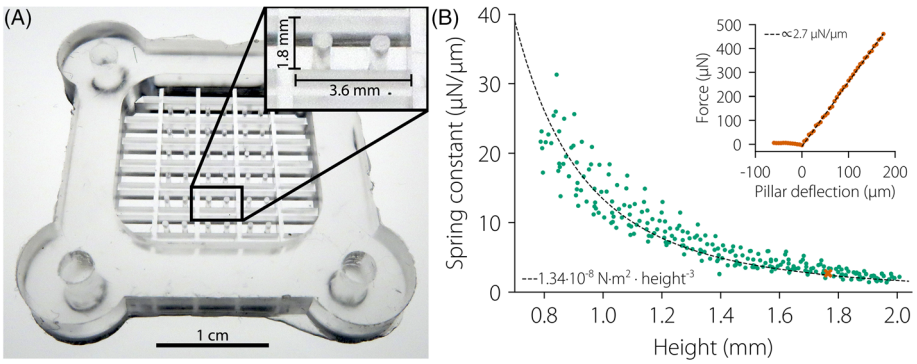

FIGURE 1 (A) PDMS device for the culture of muscle micro-tissues. (B) Calibration curve for determining PDMS pillar spring constants. The spring constants of PDMS pillars were determined at different heights with respect to the bottom of the PDMS well by measuring the force required for a defined bending (pillar deflection). A representative measurement of the force–deflection relationship at a height of 1.75 mm is shown in the inset. The spring constant is then computed from the slope of the force–deflection relationship. Green data points indicate the spring constants of individual measurements at different heights. The dotted line shows the prediction of the Euler–Bernoulli beam theory, according to which the effective spring constant is proportional to the negative third power of the height

every day. Differentiation medium consisted of DMEM supplemented with 2% horse serum, 1% penicillin–streptomycin and 0.5% insulin-transferrin-selenium (Gibco, 41400, consisting of 1 g/L insulin, 0.55 g/L transferrin, and 670 ng/L sodium selenite).

Evaluation of contractile force

The axial contractile force F of a micro-tissue was measured from the pillar deflection δ using Hooke's law

$$F = k \times \delta, \quad (1)$$

where k is the spring constant of a PDMS pillar at the height of the tissue above the pillar base h_{tissue} (Figure 2B). h_{tissue} was measured by manually focusing a bright-field microscope to the tissue regions near the pillars. k was determined from the force-bending relationship measured at different heights above the pillar base, using a motorised micromanipulator (InjectMan NI2, Eppendorf AG) and a laboratory scale (Practum 64-1S, Sartorius). The force (F) versus pillar deflection (δ) relationship at different heights (h) was then fitted to the Euler-Bernoulli beam equation: $F(h) = k_0 \times \delta/(h/h_0)^3$, where h_0 is a reference height that we arbitrarily set to 1 mm, and k_0 is the spring constant of the pillars at a height of h_0. For the devices used in this study, k_0 was around 10 μN/μm. The pillar spring constant k at different heights can then be computed according to $k = k_0/(h/h_0)^3$ (Figure 1B).

For small contractile forces of the tissues, the pillar deflection δ at the tissue height is on the order of a few μm. For higher accuracy, we therefore measured the deflection δ_{top} at the top of the pillar, where the deflection is larger than at the height of the tissue h_{tissue} (Figure 2B). δ can then be computed using the Euler-Bernoulli beam theory according to

$$\delta = 2 \times \delta_{top} \times h_{tissue}/(3 \times h_{top} - h_{tissue}), \quad (2)$$

where h_{top} is the total pillar length (2.5 mm in our setup).

In the following, we distinguish between the static and the active force. Static force is defined as the pillar bending force when the myocytes are not electrically paced. It is typically measured as the lowest force between two pacing pulses at least 1 s apart. The active force is defined as the maximum contractile force exerted by the tissues above the static force in response to electrical stimulation.

Electrical stimulation

The micro-tissues were electrically stimulated via four vertical graphite electrodes (Faber Castell pencil lead type "F" with 0.5 mm diameter) that dipped approximately 3 mm into the cell culture medium. The electrodes were rectangularly arranged in two pairs, with a distance of 9 mm between the two electrodes with equal polarity, and a distance of 18 mm between the pairs of opposite polarity. The stimulation signal was a biphasic square wave pulse consisting of a positive pulse with a field strength of 10 V/cm and 5 ms duration, followed by a negative pulse with a field strength of −10 V/cm and 5 ms duration. The pulse repetition rate was either 1 Hz for single pulse mode or 100 Hz for tetanic stimulation.

Chemical stimulation

For chemical stimulation, we "skinned" the micro-tissues with 10 mg/ml saponin in an EGTA-buffered calcium-free salt solution for three minutes. The calcium-free salt solution with an osmolality of 161 mOsm/kg as measured with an osmometer (Osmomat3000, Gonotec, Berlin) contained 30 mM Hepes, 6.25 mM Mg $(OH)_2$, 30 mM EGTA, 8 mM Na_2ATP, and 10 mM Na_2CP, and the pH was adjusted to 7.0 using 1 M KOH. Then, we washed the sample in a calcium-free salt solution and measured the contractile forces of five micro-tissues. We repeated the measurement eleven times and replaced the medium with a salt solution of gradually increasing calcium concentration before each measurement. The negative decadic logarithm of the calcium concentration (pCa) ranged from 6.74 (1.82×10^{-7} M) to 4.92

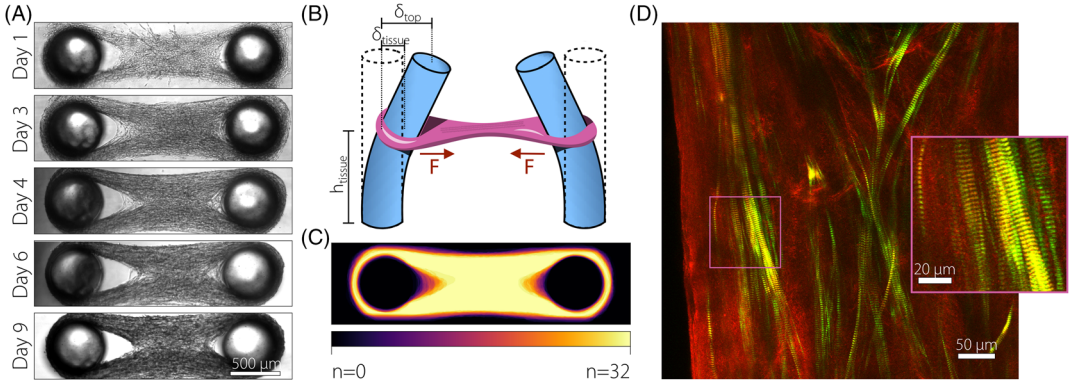

FIGURE 2 Morphology of wild-type satellite tissues. (A) Bright-field images of tissue compaction from day 1 to day 9. (B) Schematic of pillars and tissue during force generation. (C) Overlay heatmap of the morphology of 32 tissues on day 4 of differentiation. (D) SHG multiphoton confocal image of a tissue on day 21 after differentiation. Green = myosin, red = collagen

(1.19×10^{-5} M). pCa-values and contractile forces were plotted and fitted to a generalised Hill equation of the form,

$$F(pCa) = \frac{F_{max} - F_{min}}{1 + \left(\frac{EC_{50}}{pCa}\right)^{h}} + F_{min}, \quad (3)$$

where F_{min} and F_{max} are the minimum and maximum saturation levels of the Hill curve, EC_{50} is the half maximum effective concentration, and h is the Hill coefficient.

Imaging

Bright-field images were taken with a charge-coupled device camera (Hamamatsu, ORCA ER). Second harmonic generation (SHG) confocal images were taken using a multiphoton microscope (TriMScope II, LaVision BioTec) as described previously [27]. In brief, the SHG signals of myosin-II and collagen-I were excited with a Ti:Sa laser (Charmeleon Vision II, Coherent) with a power of approximately 16 mW and a pulse duration of approximately 150 fs. The backward scattered signal (405 ± 10 nm) was used for detection of fibrillar collagen. The forward scattered signal (405 ± 10 nm) was used for the detection of myosin II. The SHG signals were detected using a non-descanned transmission photomultiplier tube (H 7422–40 LV 5 M, Hamamatsu Photonics). Images were taken with a 25× dipping objective (Leica, HC Fluotar NA 0.95) with a line average of three and at a frequency of 1000 Hz. The resolution was 1024 × 1024 pixels (481.3 × 481.3 μm), and the z-stacks had a step-size of 0.5 μm.

Statistical analysis

Values are expressed as mean ± standard deviation (SD) from measurements of different micro-tissues. The statistical significance of the differences between groups (wild-type versus desmin-mutated) was assessed using a Student's two-tailed *t*-test assuming unequal variance. Boxplots indicate median values, lower to upper inter quartile values, 1.5 interquartile ranges as well as individual force measurements (as a scatter plot).

RESULTS

Formation of micro-tissues

We mixed satellite wild-type cells with unpolymerized collagen-I/Matrigel solution and seeded them in PDMS chambers containing two pillars. After the collagen-I/Matrigel solution polymerized into a fibre network, the cells started to adhere, spread, and collectively exert contractile forces. In response, the network fibres and cells aligned between the pillars. Within 24 h after seeding, the cells had compacted the fibre network into a dog bone-shaped micro-tissue (Figure 2A, "Day 1"). We then replaced the culture medium with a differentiation medium supplemented with insulin, transferrin, and selenium (ITS). Over the following days, the micro-tissues increased in width and density (Figure 2A). Typically, 4 days after seeding, the pillars started to bend inwards, indicating that the micro-tissues generated measurable contractile forces (Figure 2A,B). The morphology of wild-type micro-tissues was highly reproducible (Figure 2C). A heat map of overlaid bright-field images from 32 different micro-tissues after 4 days of differentiation (5 days after seeding) showed only slight differences in tissue morphology around the fusion region of the two tissue branches that wrap around the pillars. Second harmonic generation confocal images of collagen and myosin-II showed highly elongated, well aligned cells with the typical striation pattern of differentiated myofibres (Figure 2D).

Micro-tissues from wild-type satellite cells recapitulate the contractile behaviour of intact muscle

In tissues from wild-type satellite cells, we investigated static and active forces over 20 days of differentiation. Active force was measured as the change in force in response to electrical stimulation (±10 V/cm bipolar 5 ms pulses at 1 Hz), and the static force was measured as the minimum force between two electrical stimulation pulses (Figure 3A). We compared static and active forces in tissues grown from three different cell passages (Figure 3B,D). The static force was around 60–70 μN for tissues from all three passages and remained approximately constant over time. The active force was around 50 μN on average but exhibited a slightly higher variability between cell passages. Active and static forces slowly decreased over time in tissues from passage 1, whereas they slowly increased over time in tissues from passage 3 and 4. Importantly, active forces remained substantial in all tissues over a duration of 3 weeks.

To compare the force that the tissues generated in response to electrical versus chemical stimulation, we permeabilised the cell membrane with saponin and gradually increased the Ca^{2+} concentration in the medium from 6.74 to 4.92 (pCa). The total contractile steady-state force showed the typical sigmoidal dependence on pCa as reported for skinned single muscle fibres [28–30] (Figure 3C, S1). The pCa-concentration for half-maximum forces was 6.14 ± 0.12, and the maximum force was 65.3 ± 7.4 μN, similar to the active force in response to electrical excitation in these tissues (cell passage 14, after 9 days of differentiation).

R349P mutant desmin induces structural instability and altered contractile behaviour

We next tested the morphology and contractile performance of micro-tissues generated using satellite cells from $Des^{wt/R349P}$ mice. These tissues compacted similarly fast and were morphologically comparable to wild-type tissues at early time points. However, after around day 3 of differentiation, $Des^{wt/R349P}$ tissues started to

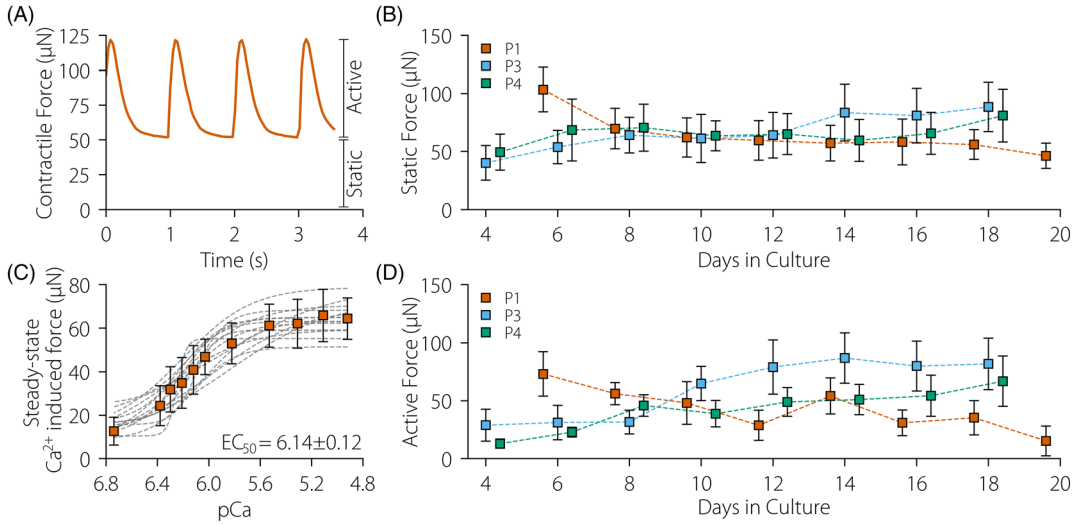

FIGURE 3 Static and active contractile forces in wild-type satellite cell tissues. (A) Static force and active contractile force in response to electrical stimulation in a representative wild-type tissue (day 10 of differentiation). (B) Static force (mean ± SD) from day 6 to day 20 of differentiation in tissues derived from three different cell passages, with number of tissues n(P1) = 18, n(P3) = 21, and n(P4) = 17. (C) Dependence of the contractile force (mean ± SD of 15 tissues) on calcium concentration in "skinned" micro-tissues. Grey lines represent the contractile response of individual micro-tissues. (D) Same as in Figure 3B for active forces

disintegrate. Individual muscle fibres ruptured at their thinnest points near the pillar, resulting in progressive cell aggregation in the central region of the tissue (Figure 4A). A heat map of bright-field images from 21 different micro-tissues after 4 days of differentiation showed a pronounced variability in tissue morphology (Figure 4B). Notably, on day 6, about two thirds of *Des*$^{wt/R349P}$ tissues had ruptured, whereas no wild-type tissue had ruptured at this time point.

We also observed substantial differences in the contractile behaviour of wild-type versus desmin-mutated tissues. The duration of a single pulse contraction (twitch) was considerably shorter in *Des*$^{wt/R349P}$ tissues (Figure 4C). From a fit of two superimposed exponential functions to the force-time trace, we found that the time constant for the force increase in response to an electrical pulse was similar (61 ± 28 ms for wild-type and 77 ± 30 ms for mutated tissues, mean ± SD, Figure 4D). However, the time constant for force relaxation was 4-times lower in the mutated tissues (79 ± 15 ms) compared with wild-type tissues (301 ± 147 ms). In addition, on day 4 of differentiation, *Des*$^{wt/R349P}$ tissues showed lower static contractile forces (26.7 ± 16.5 µN) compared with wild-type tissues (40.3 ± 23.0 µN) (Figure 4E). These differences in static force were even more pronounced on day 6 of differentiation with 28.3 ± 18.5 µN in mutated tissues compared with 110.6 ± 29.4 µN in wild-type tissues. By contrast, on day 4 of differentiation, *Des*$^{wt/R349P}$ tissues generated significantly (p < 0.01) higher active forces (40.3 ± 23.0 µN) compared with wild-type tissue (22.5 ± 4.1 µN).

The relative variability in the active force between the individual tissues, as quantified by the coefficient of variance (COV), was also considerably larger in mutated tissues (0.57) compared with wild-type tissues (0.18). The differences in active force diminished after day 6 of differentiation (62.8 ± 53.2 µN in *Des*$^{wt/R349P}$ tissues versus 60.8 ± 21.9 µN in wild-type tissues), but the variability of active forces between individual tissues remained larger in *Des*$^{wt/R349P}$ tissues (0.85) compared with wild-type tissues (0.36). Together, these data demonstrate that heterozygous knock-in of *Des*^{R349P} is associated with an increased active contractile force generation, but with reduced static tissue forces and impaired tissue integrity.

Tetanic stimulation causes rupture of desmin-mutated tissues

We next tested the hypothesis that the progressive rupture of *Des*$^{wt/R349P}$ tissues was driven by larger contractile forces. We reasoned that in combination with thinner tissue fibres that wrap around the pillars, larger forces may lead to considerably higher mechanical stress and ultimately tissue failure. To test this idea, we applied tetanic electrical stimulation (100 Hz pulse trains for several seconds), which led to 1.75 fold higher active force generation compared with single twitch stimulation, both in *Des*$^{wt/R349P}$ and wild-type tissues (Figure 5A,C; Videos S1, S2, and S3). While none of the wild-type tissues showed signs of rupture during or after tetanic stimulation, two of the four mutated tissues ruptured during tetanic stimulation. Furthermore, we observed rupture of individual fibres in the mutated tissues that survived tetanic stimulation (Videos S2 and S3).

Immediately following tetanic stimulation, single-twitch active forces were lower in both tissue types (Figure 5A). Within 5 min of continuous single twitch stimulation, however, active forces of the wild-type tissues recovered, and in some tissues even increased beyond pre-tetanus levels (106 ± 79 µN after 5 min, compared with

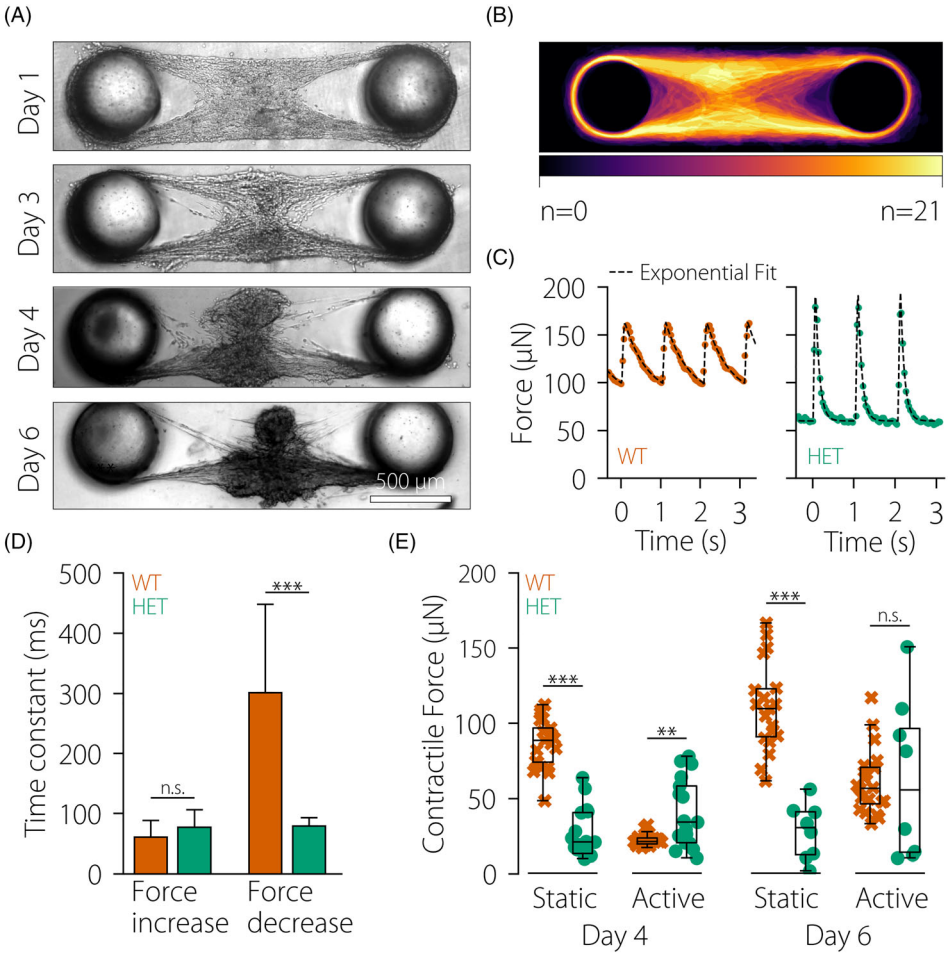

FIGURE 4 Morphology and force generation in tissues with a heterozygous desmin mutation. (A) Bright-field images of tissue compaction from day 1 to day 6 of differentiation. (B) Overlay heatmap of the morphology of 21 tissues on day 4 of differentiation. (C) Force vs. time in a typical wild-type (orange) and $Des^{wt/R349P}$ (green) tissue after 6 days of differentiation. Dots represent measurement points and dotted lines represent the superposition of two exponential functions with a short time constant for phases with increasing forces and a longer time constant for phases with decreasing forces. (D) Time constants for force increase and force decrease (mean ± SD) in wild-type (orange, $n = 19$) and $Des^{wt/R349P}$ (green, $n = 9$) tissues after 6 days of differentiation. (E) Active and static force of wild-type (orange) and $Des^{wt/R349P}$ (green) tissues on day 4 and day 6 of differentiation. $^{*}p \leq 0.05$, $^{**}p \leq 0.01$, $^{***}p \leq 0.001$, n.s., not significant ($p > 0.05$)

57 ± 14 µN prior to tetanic stimulation). We could not test how active forces recovered in *Des*$^{wt/R349P}$ tissues, as one of the two only tissues that survived after tetanic stimulation ruptured during the following single-twitch period. Static forces in wild-type tissues were not altered after tetanic stimulation (119 ± 35 µN before tetanic stimulation versus 112 ± 25 µN after 5 min; Figure 5B). The single remaining *Des*$^{wt/R349P}$ tissue, however, also showed no loss of static force. Together, these data suggest that the impaired integrity of *Des*$^{wt/R349P}$ tissues and their increased tendency to rupture is caused by excessive mechanical tension induced by hypercontractility.

$Des^{wt/R349P}$ tissues show pronounced spontaneous, inhomogeneous contractions

In the absence of electrical stimulation, wild-type tissues were quiescent and did not display spontaneous contractions. In contrast, *Des*$^{wt/R349P}$ tissues contracted spontaneously, even during the periods between two single pulses applied at 1 Hz (Video S2). These unsynchronised spontaneous contractions became particularly apparent in muscle fibres that were detached from the main tissues and accumulated in the central tissue regions. Because these muscle fibres no longer experience any appreciable load, their spontaneous contractions result in large deformations. To visualize these local deformations, we calculated the coefficient of temporal variation (COV) of pixel intensities from bright-field image sequences recorded at 28 Hz during single twitch stimulation, tetanic stimulation, and during phases without electrical stimulation ("resting") (Figure 5D). A higher COV is represented in Figure 5D with brighter colours and corresponds to larger contractile movements.

In the absence of electrical stimulation (resting phase), wild-type tissues displayed a coefficient of variation close to zero due to the lack of tissue movement, while for *Des*$^{wt/R349P}$ tissues, the spontaneous contraction across the tissue caused irregular movements and thus, a high coefficient of variation. During single twitch stimulation (1 Hz), wild-type tissues displayed a small coefficient of variation, indicating a homogenous contraction throughout the entire tissue, whereas *Des*$^{wt/R349P}$ tissues showed a high coefficient of variation, demonstrating that the tissue strain was spatially highly variable, pointing to the presence of substantial shear forces between regions of different strain. During the plateau phase of tetanic stimulation, both wild-type and *Des*$^{wt/R349P}$ tissues showed a low coefficient of variation and, hence, almost no movement as they remain in a maximally contracted state. These results indicate the presence of considerable spontaneous, unloaded contractile activity in *Des*$^{wt/R349P}$ tissues.

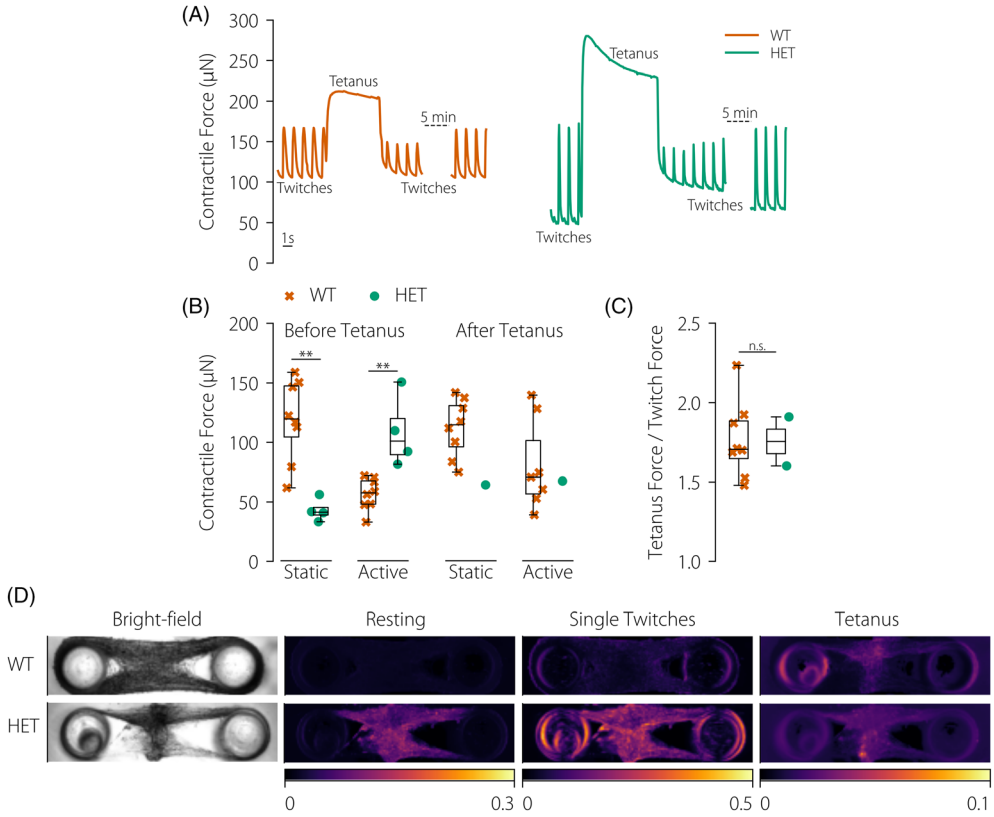

FIGURE 5 Comparison of wild-type and heterozygous desmin-mutated tissues. (A) Representative force curve of wild-type tissue (orange) compared with $Des^{wt/R349P}$ tissue (green) during single pulses and tetanic stimulation. (B) Active and static contractile force (single pulse) of wild-type and heterozygous tissues before and 5 min after tetanic stimulation. Note that two of the four mutated tissues ruptured during tetanic stimulation. (C) Ratio of maximum force increase during tetanic stimulation relative to active force during single pulse stimulation. (D) Visualization of local contractile movements from the coefficient of variation in bright-field pixel intensities (left) during a resting period (5 s), a single twitch period (1 Hz frequency, 5 s), and during full tetanic activation (5 s) for a representative wild-type and $Des^{wt/R349P}$ tissue. Scale bar 500 μm. $^{*}p \leq 0.05$, $^{**}p \leq 0.01$, $^{***}p \leq 0.001$, n.s., not significant ($p > 0.05$)

DISCUSSION

In this study, we implemented an in vitro system for fabrication, long-term culture, and mechanical assessment of skeletal muscle micro-tissues. Micro-tissues were grown from primary satellite cells isolated from skeletal muscles of wild-type mice and mice carrying a heterozygous desmin R349P mutation.

Due to their regenerative stem-cell properties, satellite cells are ideal for skeletal tissue engineering [31]. However, there are conflicting reports as to whether satellite cells can maintain their stem cell potency under culture conditions. Stem cell potency has been reported to decline within a few days after transferring isolated satellite cells into 2-D cell culture [32–34]. By contrast, culturing satellite cells in 3-D micro-tissues resulted in the maintenance of a functional satellite cell subpopulation (as revealed by staining of Pax7) for at least 2–3 weeks, even though the cells had been expanded under 2-D culture conditions for up to 5 days after isolation [35].

In our study, we generated micro-tissues from cells that had been cultured and repeatedly passaged under 2-D conditions for considerably longer than 5 days before transferring them into a 3-D culture system. We found no decline in the contractile performance with higher passage numbers (tested in this study up to passage 14). Our observations are also in agreement with two recent studies that have reported the successful generation of micro-tissues from murine [36] and rat satellite cells [35]. We have followed the protocol published in these studies for differentiating satellite cells into spontaneously contracting myotubes, which requires the addition of Matrigel to the collagen-I extracellular matrix. Matrigel contains high levels of laminin, which is essential for myotube differentiation [37]. Without Matrigel addition, our micro-tissues were unable to generate active tension.

Geometrically, our setup is an upscaled version of a previously published assay for growing micro-tissues from murine skeletal muscle cells of the C2C12 cell line in a PDMS culture chamber fabricated using soft lithography [20]. By contrast, our PDMS culture chambers are fabricated from a mould that has been machined with a conventional milling machine and drill press. Accordingly, our micro-tissues are longer (1.8 mm compared with 500 μm) and wider (300–400 μm compared with 100 μm) and are grown from 5000 cells instead of 400 cells. There is no intrinsic advantage of this geometrical upscaling other than that it allows us to control the matrix density and number of seeded cells individually for each tissue.

Our micro-tissues exhibit contractile behaviour that is in many ways similar to native muscle tissues, however with a maximum tension that is 2–3 orders of magnitude smaller. We estimated the maximum tension of wild-type micro-tissues as the sum of static and active forces normalised by the cross-sectional area, which we obtain from the width of the tissues in the mid-section and assuming a circular cross-section. Typical values of muscle tension are 675 ± 123 Pa (mean $\pm$ SD, $n = 8$) during single twitch stimulation, and 871 ± 114 Pa during tetanic stimulation. Other studies reported slightly higher twitch tensions between 1 and 2 kPa for micro-tissues grown from C2C12 skeletal muscle cells [20,21], and 1.7 kPa for micro-tissues grown from satellite cells [35]. For comparison, intact *soleus* (SOL) and *extensor digitorum longus* (EDL) muscles of young/adult mice generate tetanic tensions of around 150–220 kPa (SOL) and 200–240 kPa (EDL), respectively [38–40].

Micro-tissues show a reduced force-frequency relationship compared with primary skeletal muscle, for currently unknown reasons. At a pacing frequency of 100 Hz, the contractile force of the micro-tissues increased only by a factor of around 1.7, compared with a factor of 6.7 in adult SOL fibres, a factor of 3.8 in EDL fibres [38], and a factor of 5.7 in FDB fibres [41]. Furthermore, micro-tissues generate static forces that are comparable in magnitude to the active force, whereas static forces (also called residual tension, or tonus) in isolated primary skeletal muscle fibres are largely absent. The origin of this high static force in micro-tissues is currently unclear. Static force develops in parallel to the collective compaction/remodelling of collagen and Matrigel fibres during the first 1–2 days after cell seeding and remains approximately constant thereafter; a behaviour that has also been reported by others [19,20]. Static forces always develop before the micro-tissues gain the ability to actively contract in response to electrical excitation, and for that reason, it has been suggested that the presence of static stress is a crucial factor for successful myotube differentiation and maturation [20].

Despite their significantly lower contractile tension compared with primary skeletal muscle tissue, in vitro engineered micro-tissues offer several advantages. They provide quantitative readouts of muscle tissue mechanics and contractility over a period of several weeks under controlled conditions. In contrast, dissected muscles and single fibres can only be stored for a few days and once mounted to force transducers, can only be used over a time period of several hours. Micro-tissue systems also offer higher measurement throughput, as many more samples can be obtained from a single animal, which reduces ethical concerns. The specific advantage of satellite cells as a cell source for micro-tissues is that they proliferate and differentiate into myocytes efficiently and that they can be frozen and expanded in multiple passages (at least 14 passages in our hands) without loss of contractile performance. In addition, satellite cell-derived micro-tissues offer the possibility to study myocyte differentiation processes in a multicellular 3-D environment.

The main finding of this study is that micro-tissues derived from satellite cells with a heterozygous desmin R349P mutation are prone to tissue-disintegration. This tissue disintegration recapitulates in part the progressive skeletal muscle degenerative processes in patients suffering from desminopathies [10]. Notably, mutant micro-tissues did not exhibit any contractile impairment or weakness compared with control tissues; rather, they displayed hypercontractility that led to mechanical tissue disintegration. This behaviour can be potentially explained by four distinct mechanisms:

First, mutant cells may secrete more matrix-degrading proteases or secrete less matrix proteins so that the extracellular matrix in mutant tissues is mechanically more vulnerable and ruptures more easily when the myotubes begin to generate contractile tension. Such an altered secretory behaviour of $Des^{wt/R349P}$ cells, however, has previously not been reported, and this mechanism—although it cannot be excluded—remains speculative.

Second, desmin mutated cells may exhibit reduced adhesion strength to the matrix and, therefore, detach more readily when they contract. This mechanism, however, would leave intact matrix fibres behind, whereas we see that the matrix fibres progressively thin out as the cells recoil towards the tissue centre. Moreover, magnetic tweezer measurements using fibronectin-coated beads on heterozygous murine $Des^{wt/R349P}$ myoblasts and human $Des^{wt/R350P}$ myoblasts revealed higher adhesion strength compared with their wild-type counterparts [42,43]. Therefore, we dismiss a reduced strength of individual ECM-adhesions *per se* as a potential mechanism.

Third, reports in the literature suggest that the contractile forces in $Des^{wt/R349P}$ myotubes couples to the ECM via dystrophin/dystroglycan complex- or integrin-based adhesions that are fewer and further apart [5, 44]. This may lead to a reduced structural integrity of myofibrils and a non-uniform, uneven distribution of contractile stresses, increased local tractions, and shear deformations between parallel arranged but poorly connected myotubes. Increased local tractions and shear forces in turn may lead to a rupture of matrix fibres. Indeed, in desmin-mutated micro-tissues we find that matrix components and cells first start to disappear near the wedge-shaped bifurcation towards the pillars where the largest shear stresses can be expected. Consistent with a more uneven force distribution are furthermore reports that SOL and EDL fibre bundles from $Des^{wt/R349P}$ mice disintegrate easily when strained [30,42].

Fourth, desmin mutated myotubes may be able to generate higher contractile forces compared with wild-type myotubes, which would also lead to increased local tractions and matrix rupture. Support for this notion comes from our observation that the active forces of desmin mutated tissues are larger than those of wild-type tissues. This is particularly surprising as the majority of the mutated cells are arranged in a disorganised clump near the tissue centre where they cannot contribute to the measured pillar bending. Moreover, these larger forces are generated by relatively thin bundles of muscle cells and matrix fibres and hence are transmitted across a much smaller cross section, leading to a much higher tensile stress. Mechanical load-induced matrix fibre rupture, which prevents a direct cell rupture, could also explain recent findings that desmin-mutated muscle show lower signs of acute cell damage in response to eccentric loading [45].

It is unclear why artificial micro-tissues grown from wild-type versus desmin-mutated satellite cells show these pronounced differences in their contractile behaviour whereas in vivo-differentiated muscle

tissue and muscle fibres do not. It is conceivable that wild-type micro-tissues remain in an early state of differentiation, which would explain their low contractile tension, whereas desmin mutated tissues differentiate and mature more quickly. Another explanation could be that hypercontractile fibres do occur in desmin mutated tissue in vivo, but they eventually detach from the matrix, are subsequently removed by tissue-resident macrophages, and hence escape detection.

Currently, there are still major gaps in our understanding of the mechanisms that eventually lead to long-term loss of function in desmin-mutated muscles. Bioartificial micro-tissues are far from being an ideal model system for the study of desminopathies, but our data show that they can serve as a valuable link between single cell and whole animal studies.

ACKNOWLEDGEMENTS

This work was supported by Deutsche Forschungsgemeinschaft (DFG) grants FA-336/12.1, FR-2993/23.1, HA3309/3-1, HA3309/6-1, HA3309/7-1, TRR 225 project 326998133 (subprojects A01, B08, and C02), and the Muscle Research Center Erlangen (MURCE). C.AD. was supported by a fellowship from Ecole Polytechnique. Open access funding was provided by the Projekt DEAL.

CONFLICT OF INTEREST

The authors declare that they have no conflict of interest.

ETHICS STATEMENT

All procedures involving mice were approved by the responsible authorities as described in Materials and Methods.

AUTHOR CONTRIBUTIONS

Conceptualization: RS, BF; methodology: MS, DK, CAD, WS, IT, BF; mouse model: CSC; satellite cell isolation: DH, SH; investigation: MS, DK, BR; software: DK, RCG, CAD; formal analysis: MS, DK, RCG, BF; writing original draft: MS, DK, IT, BF; supervision, admin, funding: OF, SH, RS, BF. All authors read, edited, and approved the final version of the manuscript text and figures.

PEER REVIEW

The peer review history for this article is available at https://publons.com/publon/10.1111/nan.12784.

DATA AVAILABILITY STATEMENT

The data of this study are available upon request from the corresponding author.

REFERENCES

1. Schröder R, Vrabie A, Goebel HH. Primary desminopathies. *J Cell Mol Med*. 2007;11(3):416-426.
2. van Spaendonck-Zwarts KY, van Hessem L, Jongbloed JD, et al. Desmin-related myopathy. *Clin Genet*. 2011;80(4):354-366.
3. Clemen CS, Herrmann H, Strelkov SV, Schröder R. Desminopathies: pathology and mechanisms. *Acta Neuropathol*. 2013;125(1):47-75.
4. Schröder RC, Christoph S. Desminopathies. In: *Muscle Disease: Pathology and Genetics*. 2nd ed. John Wiley & Sons, Ltd; 2013: 178-184.
5. Paulin D, Huet A, Khanamyrian L, Xue Z. Desminopathies in muscle disease. *J Pathol*. 2004;204(4):418-427.
6. Charrier EE, Asnacios A, Milloud R, et al. Desmin mutation in the C-terminal domain impairs traction force generation in myoblasts. *Biophys J*. 2016;110(2):470-480.
7. Herrmann H, Cabet E, Chevalier NR, et al. Dual functional states of R406W-desmin assembly complexes cause cardiomyopathy with severe intercalated disc derangement in humans and in knock-in mice. *Circulation*. 2020;142(22):2155-2171.
8. Milner DJ, Weitzer G, Tran D, Bradley A, Capetanaki Y. Disruption of muscle architecture and myocardial degeneration in mice lacking desmin. *J Cell Biol*. 1996;134(5):1255-1270.
9. Li Z, Colucci-Guyon E, Pinçon-Raymond M, et al. Cardiovascular lesions and skeletal myopathy in mice lacking desmin. *Dev Biol*. 1996; 175(2):362-366.
10. Clemen CS, Stöckigt F, Strucksberg KH, et al. The toxic effect of R350P mutant desmin in striated muscle of man and mouse. *Acta Neuropathol*. 2015;129(2):297-315.
11. Li ZL, Mericskay M, Agbulut O, et al. Desmin is essential for the tensile strength and integrity of myofibrils but not for myogenic commitment, differentiation, and fusion of skeletal muscle. *J Cell Biol*. 1997; 139(1):129-144.
12. Kostareva A, Sjöberg G, Bruton J, et al. Mice expressing L345P mutant desmin exhibit morphological and functional changes of skeletal and cardiac mitochondria. *J Muscle Res Cell M*. 2008;29(1):25-36.
13. Winter L, Wittig I, Peeva V, et al. Mutant desmin substantially perturbs mitochondrial morphology, function and maintenance in skeletal muscle tissue. *Acta Neuropathol*. 2016;132(3):453-473.
14. Li M, Andersson-Lendahl M, Sejersen T, Arner A. Knockdown of desmin in zebrafish larvae affects interfilament spacing and mechanical properties of skeletal muscle. *J Gen Physiol*. 2013;141(3):335-345.
15. Ramspacher C, Steed E, Boselli F, et al. Developmental alterations in heart biomechanics and skeletal muscle function in desmin mutants suggest an early pathological root for desminopathies. *Cell Rep*. 2015;11(10):1564-1576.
16. Bär H, Fischer D, Goudeau B, et al. Pathogenic effects of a novel heterozygous R350P desmin mutation on the assembly of desmin intermediate filaments in vivo and in vitro. *Hum Mol Genet*. 2005;14(10): 1251-1260.
17. Bar H, Mucke N, Kostareva A, Sjoberg G, Aebi U, Herrmann H. Severe muscle disease-causing desmin mutations interfere with in vitro filament assembly at distinct stages. *P Natl Acad Sci USA*. 2005;102(42):15099-15104.
18. Legant WR, Pathak A, Yang MT, Deshpande VS, McMeeking RM, Chen CS. Microfabricated tissue gauges to measure and manipulate forces from 3D microtissues. *Proc Natl Acad Sci U S a*. 2009;106(25): 10097-10102.
19. Boudou T, Legant WR, Mu A, et al. A microfabricated platform to measure and manipulate the mechanics of engineered cardiac microtissues. *Tissue Eng Part a*. 2012;18(9–10):910-919.
20. Sakar MS, Neal D, Boudou T, et al. Formation and optogenetic control of engineered 3D skeletal muscle bioactuators. *Lab Chip*. 2012; 12(23):4976-4985.
21. Hofemeier AD, Limon T, Muenker TM, et al. Global and local tension measurements in biomimetic skeletal muscle tissues reveals early mechanical homeostasis. *Elife*. 2021;10:e60145.
22. Vandenburgh H, Shansky J, Benesch-Lee F, et al. Drug-screening platform based on the contractility of tissue-engineered muscle. *Muscle Nerve*. 2008;37(4):438-447.
23. Shimizu K, Genma R, Gotou Y, Nagasaka S, Honda H. Three-dimensional culture model of skeletal muscle tissue with atrophy induced by dexamethasone. *Bioengineering (Basel)*. 2017;4(2):56.
24. Vandenburgh H, Shansky J, Benesch-Lee F, et al. Automated drug screening with contractile muscle tissue engineered from dystrophic myoblasts. *Faseb j*. 2009;23(10):3325-3334.

25. Afshar Bakooshli M, Lippmann ES, Mulcahy B, et al. A 3D culture model of innervated human skeletal muscle enables studies of the adult neuromuscular junction. *Elife*. 2019;8:e44530.
26. Huraskin D, Eiber N, Reichel M, et al. Wnt/beta-catenin signaling via Axin2 is required for myogenesis and, together with YAP/Taz and Tead1, active in IIa/IIx muscle fibers. *Development*. 2016;143(17):3128-3142.
27. Schneidereit D, Nübler S, Prölß G, et al. Optical prediction of single muscle fiber force production using a combined biomechatronics and second harmonic generation imaging approach. *Light Sci Appl*. 2018;7(1):79.
28. Lamb GD, Stephenson DG. Effects of intracellular pH and [Mg2+] on excitation-contraction coupling in skeletal muscle fibres of the rat. *J Physiol*. 1994;478(Pt 2):331-339.
29. Haug M, Reischl B, Prölß G, et al. The MyoRobot: aa novel automated biomechatronics system to assess voltage/Ca^{2+} biosensors and active/passive biomechanics in muscle and biomaterials. *Biosens Bioelectron*. 2018;102:589-599.
30. Haug M, Meyer C, Reischl B, et al. The MyoRobot technology discloses a premature biomechanical decay of skeletal muscle fiber bundles derived from R349P desminopathy mice. *Sci Rep*. 2019;9(1):10769.
31. Syverud BC, Lee JD, VanDusen KW, Larkin LM. Isolation and purification of satellite cells for skeletal muscle tissue engineering. *J Regen Med*. 2014;3(2):117.
32. Machida S, Spangenburg EE, Booth FW. Primary rat muscle progenitor cells have decreased proliferation and myotube formation during passages. *Cell Proliferat*. 2004;37(4):267-277.
33. Brack AS, Conboy IM, Conboy MJ, Shen J, Rando TA. A temporal switch from Notch to Wnt signaling in muscle stem cells is necessary for normal adult myogenesis. *Cell Stem Cell*. 2008;2(1):50-59.
34. Quarta M, Brett JO, DiMarco R, et al. An artificial niche preserves the quiescence of muscle stem cells and enhances their therapeutic efficacy. *Nat Biotechnol*. 2016;34(7):752-759.
35. Tiburcy M, Markov A, Kraemer LK, et al. Regeneration competent satellite cell niches in rat engineered skeletal muscle. *FASEB Bioadv*. 2019;1(12):731-746.
36. Pruller J, Mannhardt I, Eschenhagen T, Zammit PS, Figeac N. Satellite cells delivered in their niche efficiently generate functional myotubes in three-dimensional cell culture. *Plos One*. 2018;13(9):e0202574.
37. Öcalan M, Goodman SL, Kuhl U, Hauschka SD, von der Mark K. Laminin alters cell-shape and stimulates motility and proliferation of murine skeletal myoblasts. *Dev Biol*. 1988;125(1):158-167.
38. Brooks SV, Faulkner JA. Contractile properties of skeletal muscles from young, adult and aged mice. *J Physiol*. 1988;404(1):71-82.
39. Zuo L, Nogueira L, Hogan MC. Effect of pulmonary TNF-α overexpression on mouse isolated skeletal muscle function. *Am J Physiol Regul Integr Comp Physiol*. 2011;301(4):R1025-R1031.
40. Smith LR, Barton ER. Collagen content does not alter the passive mechanical properties of fibrotic skeletal muscle in mdx mice. *American Journal of Physiology-Cell Physiology*. 2014;306(10):C889-C898.
41. Rausch M, Böhringer D, Steinmann M, et al. Measurement of skeletal muscle fiber contractility with high-speed traction microscopy. *Biophys J*. 2020;118(3):657-666.
42. Diermeier S, Iberl J, Vetter K, et al. Early signs of architectural and biomechanical failure in isolated myofibers and immortalized myoblasts from desmin-mutant knock-in mice. *Sci Rep*. 2017;7(1):1391.
43. Bonakdar N, Luczak J, Lautscham L, et al. Biomechanical characterization of a desminopathy in primary human myoblasts. *Biochem Biophys Res Commun*. 2012;419(4):703-707.
44. Konieczny P, Fuchs P, Reipert S, et al. Myofiber integrity depends on desmin network targeting to Z-disks and costameres via distinct plectin isoforms. *J Cell Biol*. 2008;181(4):667-681.
45. Langer HT, Mossakowski AA, Avey AM, et al. A mutation in desmin makes skeletal muscle less vulnerable to acute muscle damage after eccentric loading in rats. *Faseb j*. 2021;35(9):e21860.

SUPPORTING INFORMATION

Additional supporting information may be found in the online version of the article at the publisher's website.

How to cite this article: Spörrer M, Kah D, Gerum RC, et al. The desmin mutation R349P increases contractility and fragility of stem cell-generated muscle micro-tissues. *Neuropathol Appl Neurobiol*. 2021;1-11. doi:10.1111/nan.12784